Journal of the European Ceramic Society 20 (2000) 2101–2114

Processing effect on microstructure and superconducting properties of sintered $ReBa_2Cu_3Oy$ ceramics — the role of ionic radius

Constantina Andreouli [a], Athena Tsetsekou [b,*]

[a] *Ceramics and Refractories Technological Development Company (CERECO S.A.) 72nd km of Athens — Lamia Ntl. Road, PO Box 146, 34100, Chalkida, Greece*

[b] *Department of Mining Resources Engineering, Technical University of Crete, 73100, Chania, Greece*

Received 28 October 1999; received in revised form 15 February 2000; accepted 21 February 2000

Abstract

A comparison study of the processing parameters for the production of single phase sintered $ReBa_2Cu_3O_y$ samples (Re = Nd, Eu, Gd, Dy, Ho, Er), with good superconducting properties was carried out. The relationships between the microstructure of sintered $ReBa_2Cu_3O_y$ superconductors and processing variables (sintering time, sintering temperature) were examined. It was found that the superconducting properties and microstructural parameters such as density, mean grain size and the presence of secondary phases are strongly dependent upon the processing conditions and the Re-ion size of the $ReBa_2Cu_3O_y$ systems.

Keywords: Grain growth; Grain size; $ReBa_2Cu_3O_y$ systems; Sintering; Superconductors

1. Introduction

It is generally acknowledged that for large-scale applications such as permanent magnets,[1] superconducting ceramics must be processed so that they possess sufficient density to achieve reasonable mechanical behaviour without any compromise in the superconducting properties. Understanding the effects of processing conditions on the microstructure of bulk $ReBa_2Cu_3O_y$ ceramics is essential for improving the superconducting and mechanical properties.

Most of the reported works are referred to the production of $ReBa_2Cu_3O_y$ single crystals and especially to those of $NdBa_2Cu_3O_y$, using the melt process.[2–4] The control of grain size is a significant factor in determining the properties of polycrystalline $YBa_2Cu_3O_{7-x}$.[5] Grain growth mechanisms and certain transport properties have been found to vary with sintering conditions, while other properties such as T_C and the width of the superconducting transition range are virtually unaffected by the microstructural variations.[5]

Small quantities of unreacted raw materials CuO or $BaCO_3$ can dramatically affect the samples' grain growth. Aselage et al.[6] reported that small amounts of CuO increase densities and grain sizes by producing liquid phases at temperatures below the melting temperature of the stoichiometric $YBa_2Cu_3O_y$ phase, while Baik et al.[7] reported that one of the most critical steps controlling the final microstructure during sintering is the decomposition of $BaCO_3$. Hill et al.[8] have studied the relationships between the microstructure of sintered $YBa_2Cu_3O_{6+x}$ superconductors and processing variables (sintering time, sintering temperature and oxygen partial pressure). They reported that sintering of $YBa_2Cu_3O_{7-x}$ in a PO_2 of 100 kPa causes larger grains than sintering in the lower pressure of 2 kPa.

Although the relationships between processing and microstructure properties for bulk $YBa_2Cu_3O_y$ superconductors have been widely discussed and studied,[6,8–11] the investigation concerning bulk $ReBa_2Cu_3O_y$ (Re = Nd, Eu, Gd, Dy, Ho, Er) samples is not so extensive. Stepien-Damm et al.[12] reported that single-phase and high-density (90% of the theoretical one) samples of $EuBa_2Cu_3O_7$ and $GdBa_2Cu_3O_7$ were synthesized at 950°C following a two stage procedure. Using appropriate proportions of Re_2O_3, $BaCO_3$ and CuO, in a first reaction stage, a mixture of $ReBa_2Cu_3O_7$ and $BaCuO_2$ was obtained. In a second reaction stage compacts consisting of this mixture and appropriate

* Corresponding author. Fax: +30-821-69409.

0955-2219/00/$ - see front matter
PII: S0955-2219(00)00074-1

quantities of CuO and Re_2O_3 had undergone strong densification due to a transient formation of a eutectic phase between $BaCuO_2$ and CuO. Yao et al.[2] investigated the growth rate and the superconducting properties of large $ReBa_2Cu_3O_y$ single crystals and reported that, for the $ReBa_2Cu_3O_y$ systems with large-ionic radius Re elements (e.g. $NdBa_2Cu_3O_y$), the Re element may enter at the Ba site under high oxygen partial pressure leading to lower critical temperature T_C.

The aim of this work is to investigate the preparation routes (the processing parameters) for the production of single phase sintered $ReBa_2Cu_3O_y$ samples (Re: Nd, Eu, Gd, Dy, Ho, Er), with good superconducting properties. The relationships between the microstructure of sintered $ReBa_2Cu_3O_y$ superconductors and processing variables (sintering time, sintering temperature) were examined. X-ray diffraction analysis was applied to characterise these samples and SEM, coupled with EDS analysis, were used in order to examine their microstructure. Superconducting properties and microstructural parameters such as density, mean grain size and the presence of secondary phases are strongly dependent upon the processing conditions and the Re-ion size of the $ReBa_2Cu_3O_y$ systems.

2. Experimental

The $ReBa_2Cu_3O_y$ (Re = Nd, Eu, Gd, Dy, Ho, Er) powders were synthesised via a multi-step solid state reaction process using as raw materials Re_2O_3 (Micropure products, 99.99% purity), $BaCO_3$ and CuO (Alfa products, 99.999% purity). All rare earth oxides exhibited similar particle size distributions showing a mean value at about 7 μm, while the 90% of the powders were under 15 μm. The final powders were produced after calcination at 900°C for a total time of 35 h. The calcination procedure comprised four steps, with the exception of the $ErBa_2Cu_3O_y$ system that required an extra calcination step at 900°C for an additional period of 10 h. The experimental procedure as well as all the derived results concerning the synthesis of $ReBa_2Cu_3O_y$ powders is reported in detail elsewhere.[13] The above final powders were characterized by X-ray diffraction analysis (SIEMENS D-500 X-Ray diffractometer, CuK_α radiation) and particle size distribution measurements (Malvern 3600E particle size analyser). These powders were shaped into cylindrical samples (15 mm diameter, 5 mm height) by cold isostatic pressing (National Forge Europe) at 300 MPa.

In order to further investigate the green sample behaviour during calcination, DTA analysis was carried out in a Pt crucible, under flowing oxygen, up to a temperature of 1050°C with a heating rate of 2°C/min. Their densification behaviour during sintering was investigated by carrying out dilatometric measurements in a Netzsch-DIL 402C instrument (heating rate 2°C/min, final temperature 990°C and oxygen atmosphere). The pellet specimens were placed on $BaZrO_3$ plates and were sintered in an oxygen atmosphere under various firing conditions, in order to optimise the thermal cycle for each powder system. The sintering temperature was varied between 910 and 1000°C and the dwell time between 6 and 20 h. The heating rate was 2°C/min and the cooling rate 1°C/min. All the samples were annealed during cooling at 450°C for 20 h.

The apparent density of sintered specimens was measured by the Archimedes method using cycloexanone as the liquid medium. The produced samples were characterised by X-ray diffraction analysis and their microstructure was studied using combined scanning electron microscopy (SEM) (JEOL 6300) and energy dispersive X-ray microanalysis (EDS) (LINK ISIS). Grain sizes were measured directly from the micrographs using the method reported by Gotor et al.[14] The average grain size included measurements of approximately 200 individual grains and was obtained from the arithmetic average between width and length size. The electrical resistance of the samples was measured from room temperature to 77 K, using the four-point technique.

3. Results

3.1. $ReBa_2Cu_3O_y$ powder analysis

All the powders synthesized via the multi-step-solid state reaction process described in detail elsewhere,[13] exhibited almost the same particle size distribution (90% under 14 μm, 10% under 3 μm), as it is clearly observed in Fig. 1. X-ray diffraction analysis (Fig. 2) of the final powders produced by this method showed that they are quite pure, containing the $ReBa_2Cu_3O_y$ orthorhombic phase (<123>) and some traces of the secondary phases $BaCuO_2$ (<011>), Re_2BaCuO_5 (<211>) and CuO. However, it was observed that the purity of the powders differs among the powder systems depending on the ionic radius of the rare earth (Re) ion present in the system. Thus, the powder systems with lower ionic radius than that of Dy ($r_{Re} \leqslant r_{Dy}$) contained along with the $ReBa_2Cu_3O_y$ phase, detectable amounts of the secondary phases Re_2BaCuO_5 and $BaCuO_2$. This behaviour was more intense for the ErBCO system. Although it required an extra calcination step for the orthorhombic phase $ErBa_2Cu_3O_y$ to be completely formed, it contained (along with the $ErBa_2Cu_3O_y$ phase) higher amounts of Er_2BaCuO_5 phase, compared to the other powder systems (Fig. 2).

The results of simultaneous TG-DTA experiments that were carried out on $ReBa_2Cu_3O_y$ powders under flowing oxygen are shown in Table 1. In Fig. 3, the DTA curve of one of these systems, HoBCO that heated

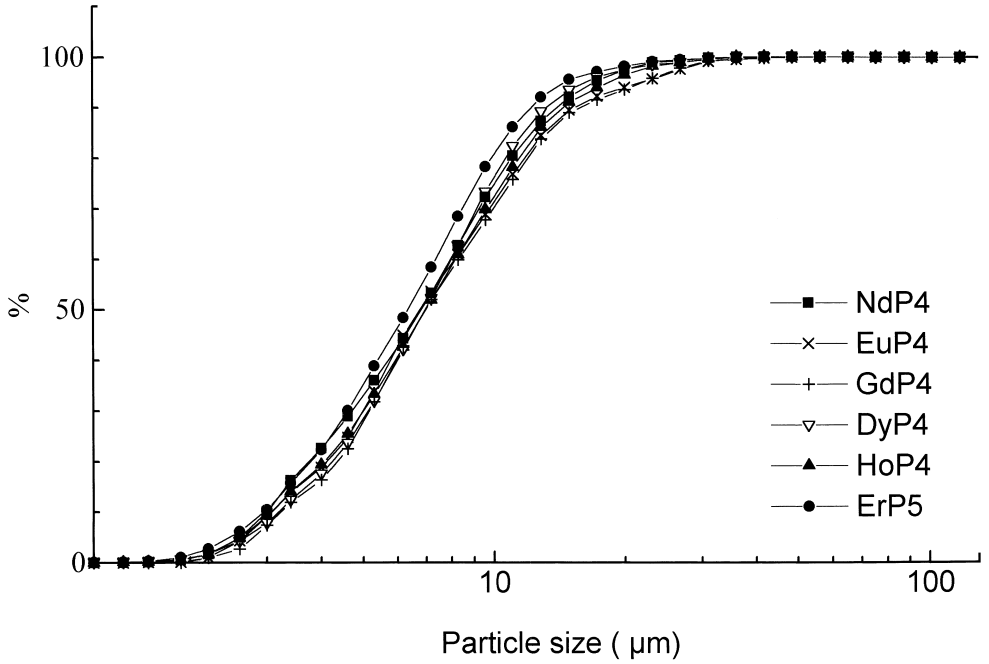

Fig. 1. Particle size distribution of the final $ReBa_2Cu_3O_y$ powders used for the production of dense samples.

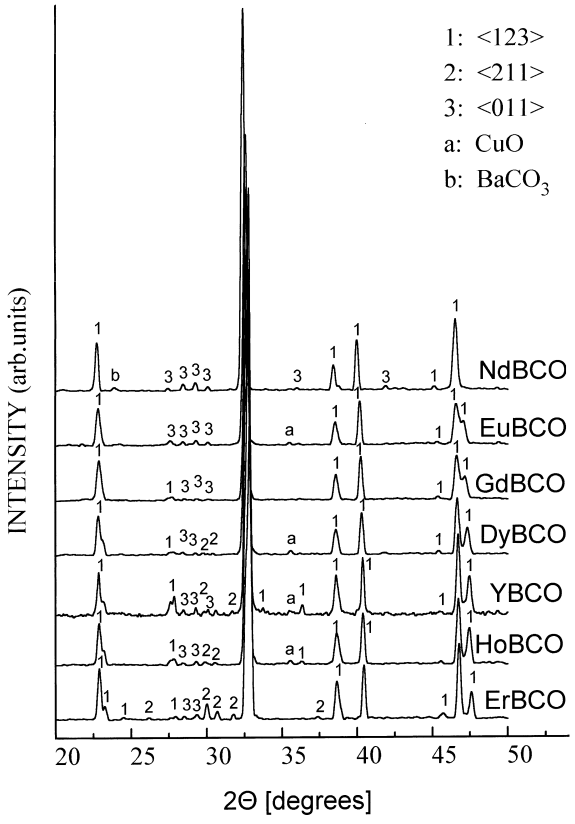

Fig. 2. X-ray diffraction analysis of $ReBa_2Cu_3O_y$ powders produced from a four step calcination procedure at 900°C for 35 h.

under O_2 atmosphere with a heating rate of 2°C/min, is presented. Most of the systems exhibited an endothermic event at around 940–960°C. From Fig. 2, it can be clearly seen that XRD analysis could detect CuO impurities in all the systems (with the exception of ErBCO), which presented this endothermic peak. On the other hand, in the systems where DTA results did not show this event (NdBCO and GdBCO), CuO impurities could not be detected.

Table 1
Results from thermogravimetric analysis

ReBCO system	Temperature of endothermic events (°C)		
	1st Endotherm	2nd Endotherm	Melting
NdBCO	–	–	1032
EuBCO	943	–	1035
GdBCO	–	–	1007, 1022, 1048
DyBCO	937	–	1024
YBCO	956	–	1025
HoBCO	952	970	1040
ErBCO	954	968	994

3.2. Densification behaviour of $ReBa_2Cu_3O_y$ samples

The densification behaviour of the $ReBa_2Cu_3O_y$ powders was investigated by carrying out dilatometric measurements. The curves of the samples' shrinkage and shrinkage rate (1st derivative of the shrinkage curve) as a function of temperature are presented in Fig. 4. The results showed that for all powders the shrinkage starts between 855 and 905°C depending on the powder system. Shrinkage rate curves showed that the temperature of maximum shrinkage, which lies in the range 925–941.5°C, depends again on the powder system (Table 2). The systems of smaller ionic radius of the central ion Re, show steeper shrinkage curves and lower

temperatures of maximum shrinkage. $DyBa_2Cu_3O_y$ system is very characteristic, from the point of view of a very abrupt densification curve starting at the lowest temperature of 855°C. On the contrary, the $NdBa_2Cu_3O_y$ sample was densified with difficulty, with the curve being shifted towards the highest temperature of 905°C.

It is worth noting that $HoBa_2Cu_3O_y$ is the only sample that exhibits two distinct peaks in the shrinkage rate curve (Fig. 4b). The first peak was at 929°C and the second one at 948°C. However, the other $ReBa_2Cu_3O_y$ samples exhibited only one peak in this curve.

Since dilatometric measurements showed that the densification for almost all $ReBa_2Cu_3O_y$ powders occurs in the temperature range 930–980°C, sintering studies were carried out in the region 910–1000°C. The effect of sintering temperature on the density of the examined $ReBa_2Cu_3O_y$ samples, sintered under O_2 atmosphere, for 6 hours is shown in Fig. 5. At the low sintering temperature of 910°C, all the $ReBa_2Cu_3O_y$ samples exhibited densities in the range 75–84% of the theoretical one. At this temperature, $NdBa_2Cu_3O_y$ and $EuBa_2Cu_3O_y$ samples exhibit low-density values while the $GdBa_2Cu_3O_y$ samples present much higher density. By increasing the sintering temperature, the density of $NdBa_2Cu_3O_y$, $EuBa_2Cu_3O_y$ and $GdBa_2Cu_3O_y$ samples increases almost linearly, following a different rate for

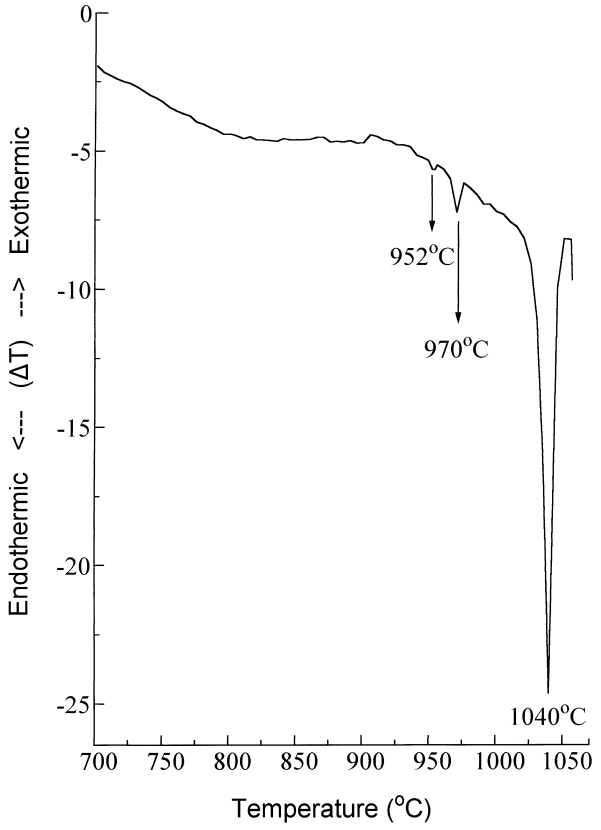

Fig. 3. DTA heating curve of a $HoBa_2Cu_3O_y$ green sample heated under O_2 atmosphere with a heating rate of 2°C/min.

Table 2
Results from dilatometric measurements

ReBCO system	Onset temperature of shrinkage (°C)	Temperature of maximum shrinkage rate (°C)
NdBCO	905	941.5
EuBCO	885	930
GdBCO	878	926
DyBCO	855	930
HoBCO	872	929, 948
ErBCO	865	925

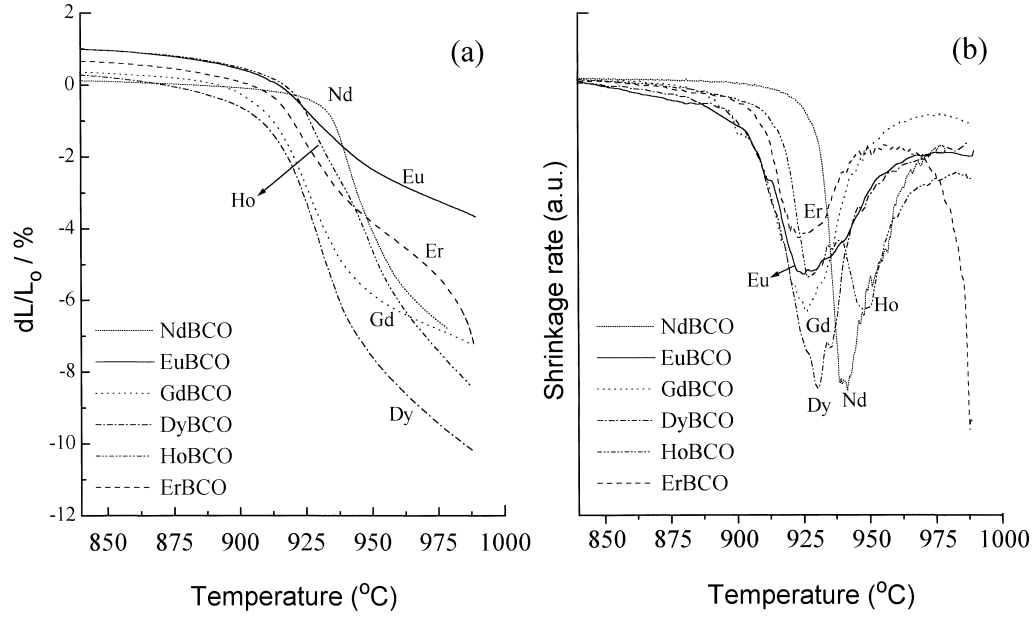

Fig. 4. (a) Linear sintering shrinkage and (b) shrinkage rate of $ReBa_2Cu_3O_y$ samples as a function of sintering temperature.

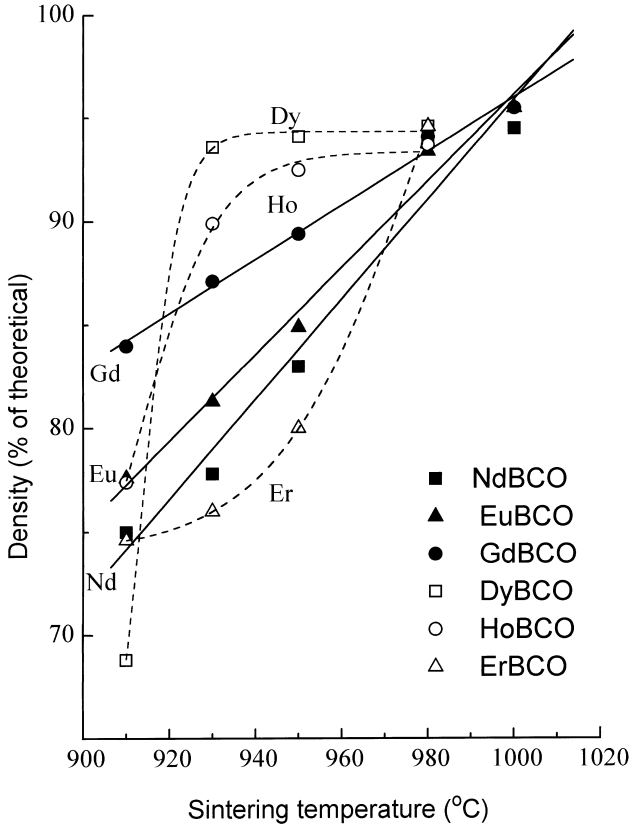

Fig. 5. Densities of $ReBa_2Cu_3O_y$ samples (% of the theoretical one) sintered for 6 h at various sintering temperatures.

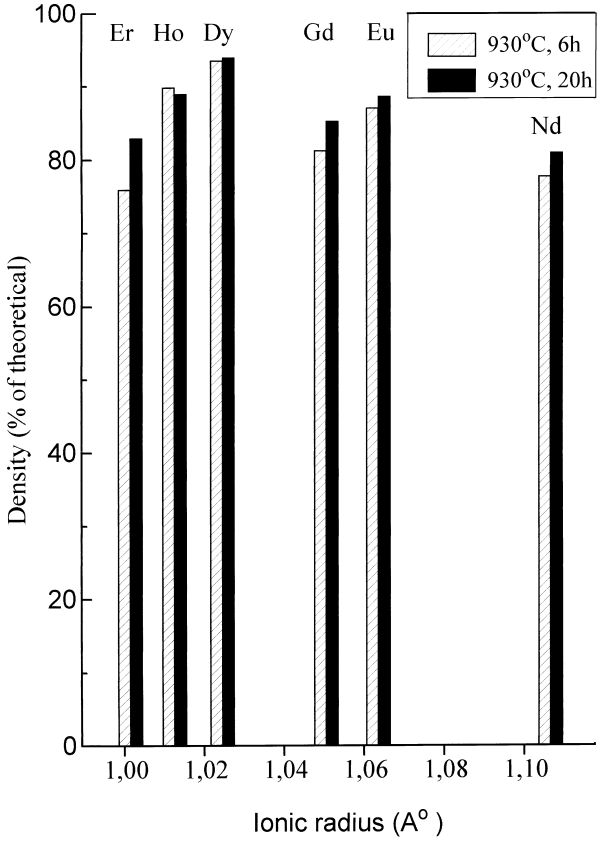

Fig. 6. Densities of $ReBa_2Cu_3O_y$ samples (% of the theoretical one) sintered at various temperatures for 6 or 20 h, as a function of the Re ionic radius.

each one. On the contrary, the density of $DyBa_2Cu_3O_y$, $HoBa_2Cu_3O_y$ and $ErBa_2Cu_3O_y$ samples, which have smaller central ion Re, exhibit a different behaviour. Their density, in accordance to dilatometric measurements, presents an abrupt increase at a specific temperature. For the specimens of $ErBa_2Cu_3O_y$ system with the lower Re ion size, the density increases very slowly as the sintering temperature increases from 910 to 950°C showing low values, lower than 80% of the theoretical density, while at 950°C an abrupt increase is observed. For $DyBa_2Cu_3O_y$ and $HoBa_2Cu_3O_y$ samples, the densification is more abrupt. Especially the $DyBa_2Cu_3O_y$ sample reaches its maximum density, which is 94% of the theoretical one, at the temperature of 930°C, whereas $HoBa_2Cu_3O_y$ sample at 930°C densifies also abruptly reaching a density of 90% of the theoretical one. For higher sintering temperatures its density continues to increase with a slower rate, reaching its maximum value after sintering at 980°C. The influence of sintering time on densification is less significant (Fig. 6). Increasing the sintering time from 6 to 20 h (for the intermediate sintering temperature of 930°C), the density of the $ReBa_2Cu_3O_y$ samples did not significantly change. Only the $ErBa_2Cu_3O_y$ sample exhibited a higher density increase in this case.

Thus, at the high enough temperature of 980°C the samples of all six systems have reached their maximum density, which is about 95% of the theoretical one, while further increase of the sintering temperature does not improve anymore the sample density.

3.3. X-ray diffraction measurements of $ReBa_2Cu_3O_y$ samples

X-ray diffraction analysis was employed to determine the quality of the sintered samples and the X-ray diffraction patterns are shown in Fig. 7. For the samples $NdBa_2Cu_3O_y$, $EuBa_2Cu_3O_y$ and $GdBa_2Cu_3O_y$ with the higher Re ion size, the maximum sintering temperature was 1000°C. As it is shown in Fig. 7a–c, in all cases the samples consist only of the $ReBa_2Cu_3O_y$ phase. However, $DyBa_2Cu_3O_y$, $HoBa_2Cu_3O_y$ and $ErBa_2Cu_3O_y$ samples with the Re ion of the smaller size, at the high temperature of 1000°C reacted with the $BaZrO_3$ substrate. For this reason the analysis concerns the samples sintered in the temperature range of 910–980°C. In more details, $DyBa_2Cu_3O_y$ samples exhibit high purity in this sintering temperature range, while $HoBa_2Cu_3O_y$ samples where the Re ion size is even smaller, exhibit high purity only up to 950°C (Fig. 7d). At the higher

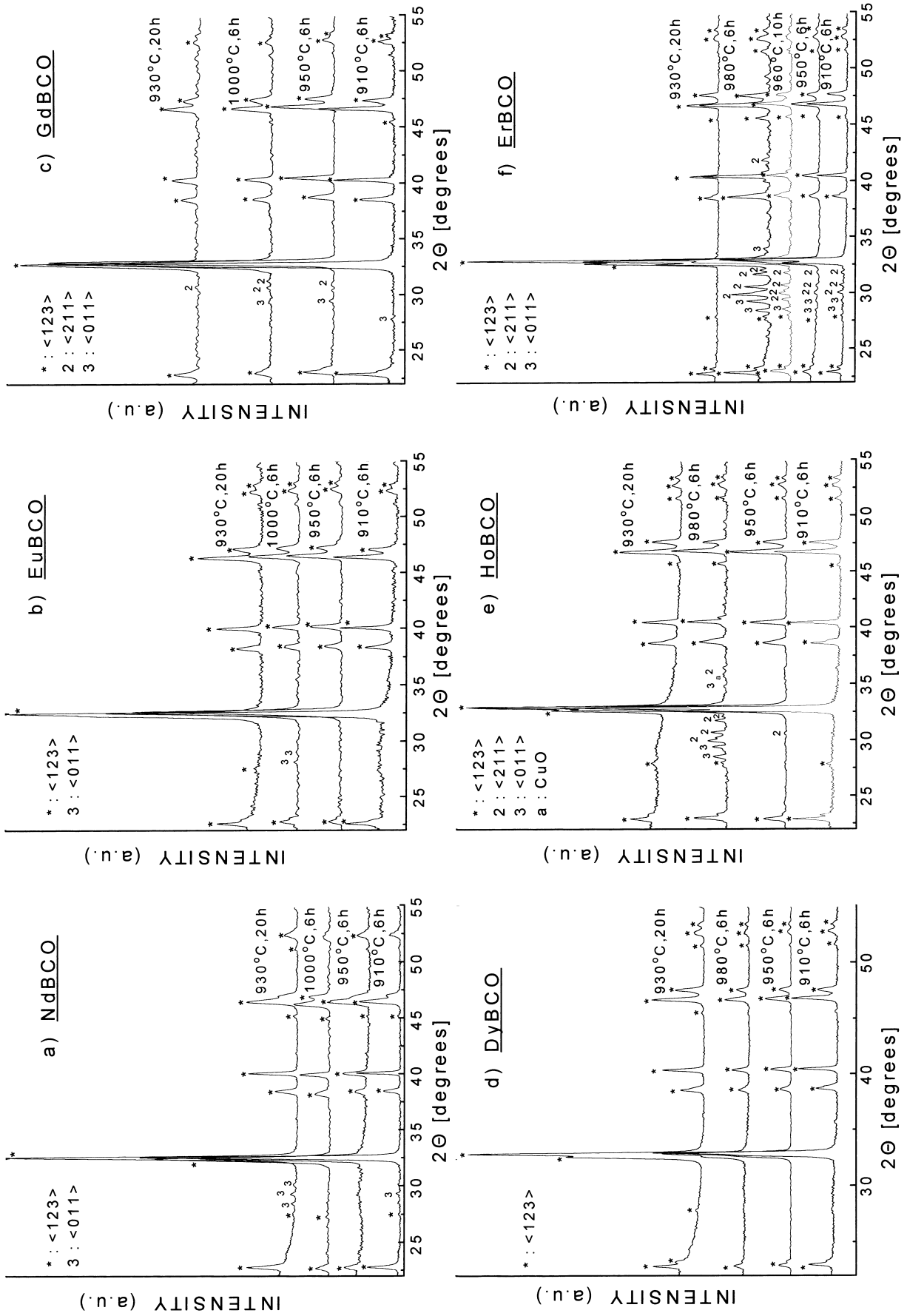

Fig. 7. X-ray diffraction analysis of $ReBa_2Cu_3O_y$ samples: (a) $NdBa_2Cu_3O_y$; (b) $EuBa_2Cu_3O_y$; (c) $GdBa_2Cu_3O_y$; (d) $DyBa_2Cu_3O_y$; (e) $HoBa_2Cu_3O_y$; (f) $ErBa_2Cu_3O_y$ sintered at various conditions with a heating rate of 2°C/min under oxygen atmosphere.

temperature of 980°C HoBCO samples contained, along with the $HoBa_2Cu_3O_y$ phase, the decomposition products Ho_2BaCuO_5 and $BaCuO_2$ (Fig. 7e). On the contrary ErBCO samples in all cases consisted, apart from the $ErBa_2Cu_3O_y$ phase of the secondary phases Er_2BaCuO_5 and $BaCuO_2$. However, an increased purity is observed as the sintering time increases. The behaviour of $ErBa_2Cu_3O_y$ samples during the sintering process is strongly correlated to the inadequate purity of the starting powder. As it has been mentioned elsewhere,[13] the systems with the smaller Re ion, exhibit slower reaction rate for the formation of the $ReBa_2Cu_3O_y$ phase and the decomposition temperature of this phase is also lower. Therefore, the ErBCO powder system with the smallest Re ion size, required an extra calcination step for the orthorhombic phase to be completely formed. Even after this additional step, the powder had showed lower purity compared to the other ReBCO powder systems, containing except of the $ErBa_2Cu_3O_y$ phase, small traces of the green phase Er_2BaCuO_5 and even smaller traces of the $BaCuO_2$ phase.

Increasing the sintering time from 6 to 20 h, the purity of the samples, according to XRD analysis (and within the detection limit of the method), remained almost unaffected, except for ErBCO system. For this system the increase of the sintering time improved sample purity by supporting the completion of the $ErBa_2Cu_3O_y$ formation reaction. Thus, after 20 h sintering no other secondary phases were detected in the samples.

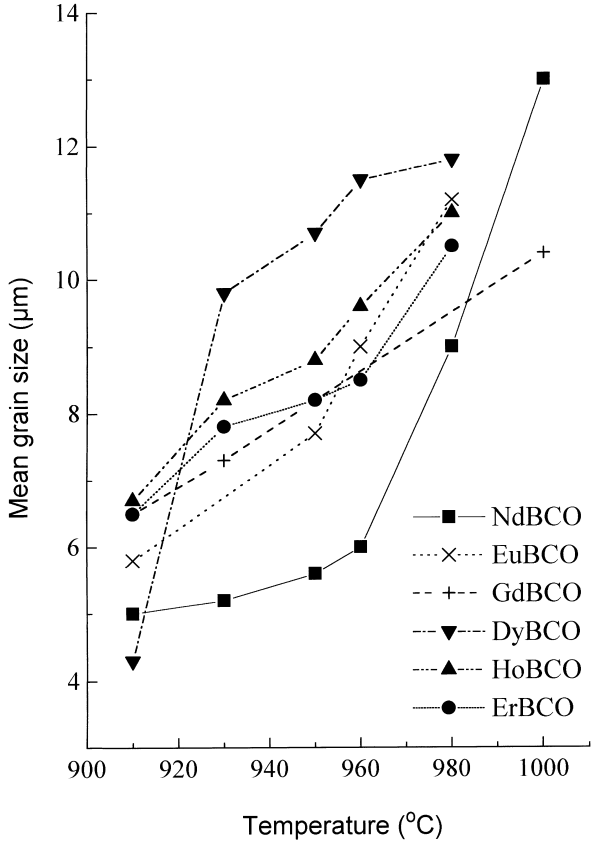

Fig. 8. Mean grain size of $ReBa_2Cu_3O_y$ samples sintered at 910, 930, 950, 970 and 980°C for 6 h.

3.4. Scanning electron microscopy/energy-dispersive x-ray analysis

The $ReBa_2Cu_3O_y$ samples sintered for 6 h at various temperatures between 910 and 980°C were examined with SEM and X-ray energy dispersive microanalysis. All the measurements were carried out on fractured surfaces. The mean grain size of the sintered $ReBa_2Cu_3O_y$ samples is plotted in Fig. 8, for different sintering temperatures and these data are in good agreement with the density data reported earlier in Figs. 5 and 6. It was observed that the denser samples exhibit larger grain sizes and the sintering behaviour of $ReBa_2Cu_3O_y$ samples was varied across the lanthanide series.

3.4.1. $NdBa_2Cu_3O_y$ samples

The $NdBa_2Cu_3O_y$ samples, sintered for 6 h at 910°C, exhibit plate-like grains with a broad size distribution and the average grain size is about 5 μm. At this temperature, no substantial grain growth was observed, since the mean grain size was comparable to the mean particle size of the powder employed. Even at the higher temperature of 930°C the mean grain size does not significantly change (Fig. 9a), however the neck growth process taking place between the particles, known as the initial stage of the sintering process, is in progress. After sintering at 950 and 960°C for 6 h the $NdBa_2Cu_3O_y$ samples consist of elongated grains (Fig. 9b) as a result of the rapid neck growth process. Substantial grain growth is observed only after 6 hours sintering at the temperature of 980°C (Fig. 9c), where the mean grain size reaches 9 μm. The grain growth process continues and at the temperature of 1000°C the mean grain size extends to 13 μm. In this case the rapid grain growth supported the pore entrapment inside the grains. These pores exhibit a size of 1–2 μm. EDS analysis showed that in all cases only grains of $NdBa_2Cu_3O_y$ phase were found.

3.4.2. $EuBa_2Cu_3O_y$ samples

Similar behaviour is observed in the $EuBa_2Cu_3O_y$ samples. The only difference between $NdBa_2Cu_3O_y$ and $EuBa_2Cu_3O_y$ samples is that the grain growth is somewhat higher, in accordance with the dilatometric measurements, which showed an earlier start of the shrinkage in this system. As a result, the $EuBa_2Cu_3O_y$ samples sintered for 6 h at 910°C, exhibit substantial grain growth and the average grain size is about 7 μm. In this case as well, EDS could not detect any impurity phases.

3.4.3. $GdBa_2Cu_3O_y$ samples

In the $GdBa_2Cu_3O_y$ samples, the results were also similar with a slightly higher grain growth rate being

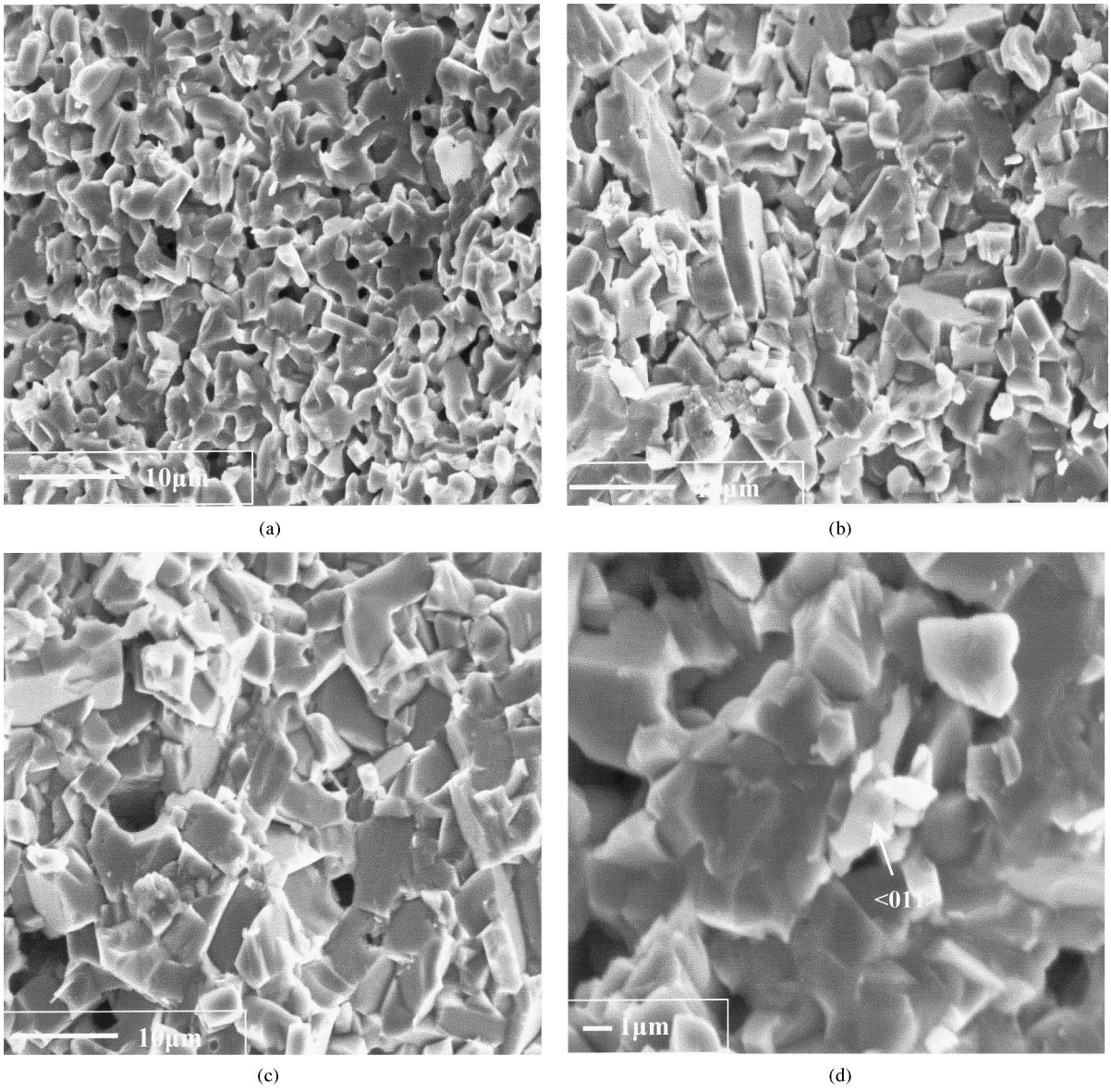

Fig. 9. SEM micrographs of $ReBa_2Cu_3O_y$ samples sintered for 6 h under O_2 atmosphere: (a) $NdBa_2Cu_3O_y$ at 930°C; (b) $NdBa_2Cu_3O_y$ at 960°C; (c) $NdBa_2Cu_3O_y$ at 980°C; (d) $GdBa_2Cu_3O_y$ at 950°C.

observed in this case. However, EDS analysis showed the presence of few dispersed particles of a foreign phase, at the grain boundaries (Fig. 9d). These particles are observed even in samples sintered at only 910°C and exhibit a mean size of 2–3 μm and have the $BaCuO_2$ composition. Perhaps their presence must be attributed to the $BaCuO_2$ impurities present in the starting $GdBa_2Cu_3O_y$ powder.

3.4.4. $DyBa_2Cu_3O_y$ samples

$DyBa_2Cu_3O_y$ samples' microstructure after sintering at 910°C for 6 h, consist of stoichiometric grains, 5–7 μm in size and a lot of needle-like grains with dimensions of 3×0.7 μm (Fig. 10a). Some of these needle-like grains grow on some unreacted CuO particles and exhibit a stoichiometry close to that of Dy_2BaCuO_5 phase. At the higher temperature of 930°C, the samples exhibit a totally different microstructure. Substantial grain growth has occurred and most of the grains present the typical plate-like form with a size of 6–7 μm. There are also some big elongated grains with dimensions 15×3–5 μm and the mean size is about 11 μm (Fig. 10b). Their grain size does not increase significantly up to 960°C, keeping a mean value at about 11.5 μm, after sintering at this temperature. At the even higher temperature of 980°C, the sample starts to have a glassy appearance (Fig. 10c), while large pores are observed.

3.4.5. $HoBa_2Cu_3O_y$ samples

$HoBa_2Cu_3O_y$ samples sintered for 6 h at 910°C consist of grains with a mean grain size of about 6 μm. Significant increase of the grains is observed for temperatures higher

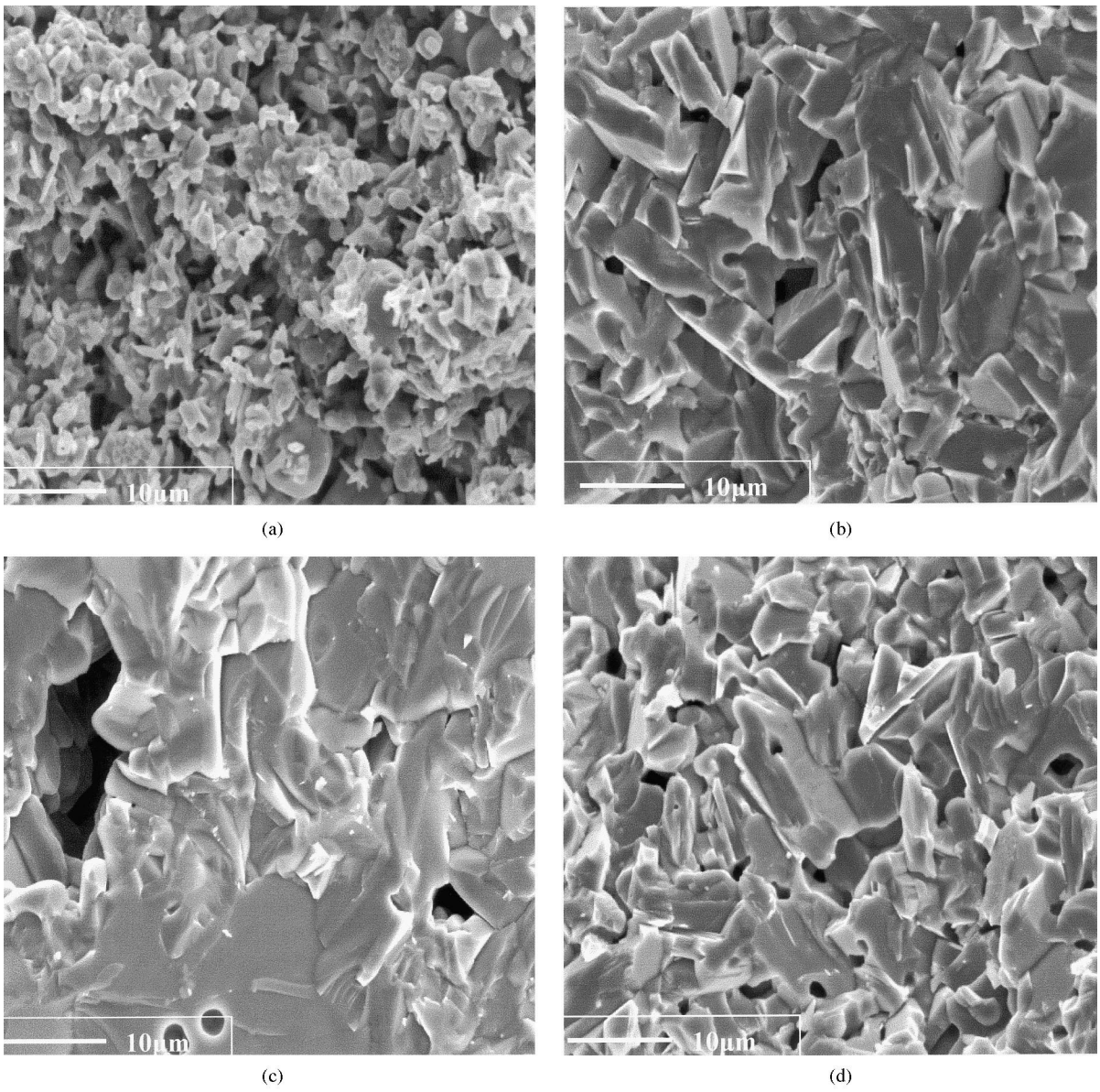

Fig. 10. SEM micrographs of $ReBa_2Cu_3O_y$ samples sintered for 6 h under O_2 atmosphere: (a) $DyBa_2Cu_3O_y$ at 910°C; (b) $DyBa_2Cu_3O_y$ at 930°C; (c) $DyBa_2Cu_3O_y$ at 980°C; (d) $HoBa_2Cu_3O_y$ at 930°C.

than 930°C (Fig. 10d). At this temperature the mean grain size increases to about 8 μm. Further increase of the sintering temperature, leads to a slight enlargement of the grains, while at the higher temperature of 980°C the sample is partially glassy and some grains exhibit stoichiometry close to $Ho_2Ba_CuO_5$ phase. $HoBa_2Cu_3O_y$ samples, which were sintered at the temperatures of 935 and 955°C for 2 h and then rapidly cooled at room temperature, were also examined in order to study the phenomenon of the change in densification rate observed in the dilatometric measurements. As it was observed from the SEM pictures of the fractured surface of these samples, the ones sintered at 955°C present a regular structure of $HoBa_2Cu_3O_y$ grains, while those sintered at the lower temperature of 935°C exhibit two distinct regions: (a) the first region has the form of a smooth melt-like layer which is rich in Ba and Cu and exhibits a stoichiometry close to the $BaCuO_2$ phase ($<011>$) and (b) the other region exhibits the correct $HoBa_2Cu_3O_y$ stoichiometry and is located close to the previously described one. This region consists of elongated needle-like grains, resulting from a rapid growth process. However, the $HoBa_2Cu_3O_y$ samples, sintered for 6 h at the temperatures of 930 and 950°C and then slowly cooled, do not present such an irregular structure.

3.4.6. $ErBa_2Cu_3O_y$ samples

The $ErBa_2Cu_3O_y$ samples present a different microstructure. The samples sintered for 6 h at 910°C

consist mainly of: (a) asymmetric or plate-like $ErBa_2Cu_3O_y$ grains, (b) some spherical grains or spherical agglomerates with stoichiometry very close to Er_2BaCuO_5 phase and (c) some smooth asymmetric grains of $BaCuO_2$ (Fig. 11a), that possess higher contrast compared to $<123>$ grains. The Er_2BaCuO_5 and $BaCuO_2$ grains observed at this temperature are attributed to the impurities of the starting $ErBa_2Cu_3O_y$ powder. Up to the temperature of 960°C, the mean grain size of the samples is less than 8 μm, while at the higher temperature of 970°C the samples are partially glassy. The $ErBa_2Cu_3O_y$ samples sintered for 6 h at the even higher temperature of 980°C consist mainly of large asymmetric or rectangular (18×7 μm) Er_2BaCuO_5 grains (Fig. 11b).

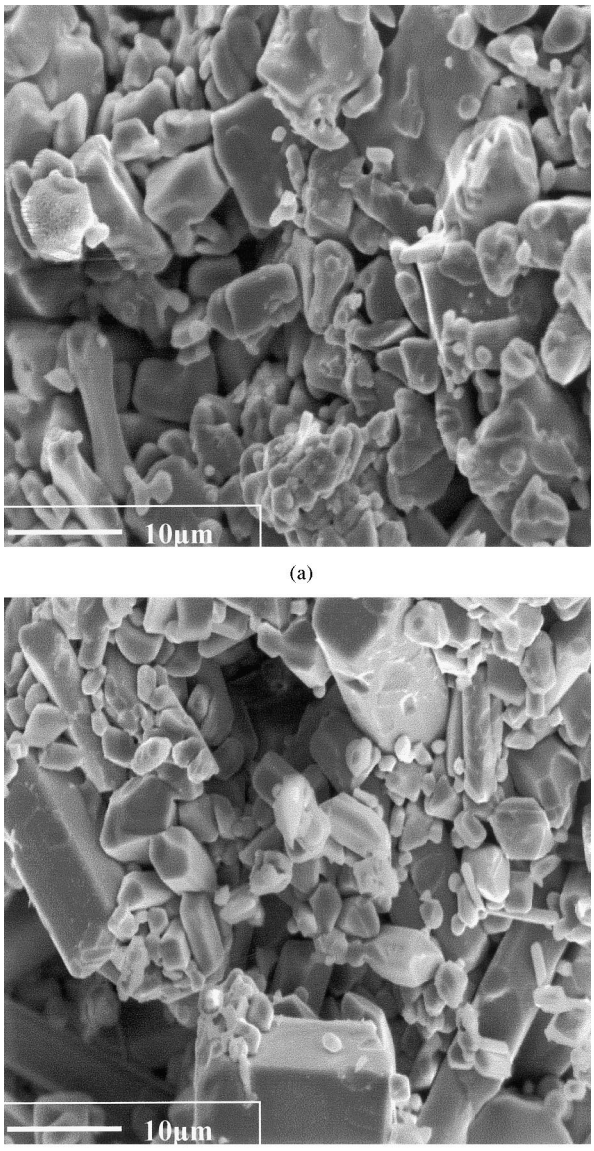

Fig. 11. SEM micrographs of $ErBa_2Cu_3O_y$ samples, sintered for 6 h under O_2 atmosphere: (a) at 910°C; (b) at 980°C.

3.5. Electrical resistance study of $ReBa_2Cu_3O_y$ samples

The superconducting critical temperature was estimated from electrical resistance measurements using the four-point technique. The results concerning the onset and the offset temperature for the superconducting transition are described in Table 3 and are plotted in Fig. 12.

The systems with low ionic radius $DyBa_2Cu_3O_y$, $HoBa_2Cu_3O_y$ and $ErBa_2Cu_3O_y$ were measured after sintering at 950°C for 6 h since at this temperature both $DyBa_2Cu_3O_y$ and $HoBa_2Cu_3O_y$ presented the highest purity and density. $ErBa_2Cu_3O_y$ ($<123>$ phase) samples did not exhibit their maximum density, but after sintering at higher temperature the $ErBa_2Cu_3O_y$ phase had undergone significant decomposition (Fig. 7). The systems with higher Re ion size $EuBa_2Cu_3O_y$ and $GdBa_2Cu_3O_y$, were measured after sintering at 980°C, which is the temperature leading to their maximum density without deteriorating their purity. In all five cases the transition temperatures were close to the optimum values referred in the literature.[15] $NdBa_2Cu_3O_y$ samples were measured after sintering at various temperatures (Table 3) but in all cases the onset of the superconducting transition was at about $T_{C_{onset}} = 77$ K and the samples were not superconducting above the liquid nitrogen temperature, as the offset temperature was at $T_{c_{offset}} = 40$ K.

4. Discussion

The stoichiometric $ReBa_2Cu_3O_y$ powders were found to contain some detectable amounts of the secondary phases Re_2BaCuO_5 and $BaCuO_2$ as well as small amounts of excess CuO, enough though to induce a small thermal event at around 940–960°C, on the DTA plot (Fig. 3).

Various studies referred to $YBa_2Cu_3O_y$ samples, report the appearance of an endothermic peak in the DTA curve at the temperature range 940–960°C attributed to the peritectic reaction of ⟨123⟩ phase with CuO impurities:[6,8,9]

Table 3
Critical temperature $T_{C_{onset}}$ and $T_{C_{offset}}$ of ReBCO samples

ReBCO samples	Sintering conditions			
	950°C, 6 h		980°C, 20 h	
	$T_{C_{onset}}$ (K)	$T_{C_{offset}}$ (K)	$T_{C_{onset}}$ (K)	$T_{C_{offset}}$ (K)
NdBCO	77	<40	78	40
EuBCO	–	–	95	84.5
GdBCO	–	–	94	88
DyBCO	93	86	–	–
HoBCO	93	90	–	–
ErBCO	93.5	90	–	–

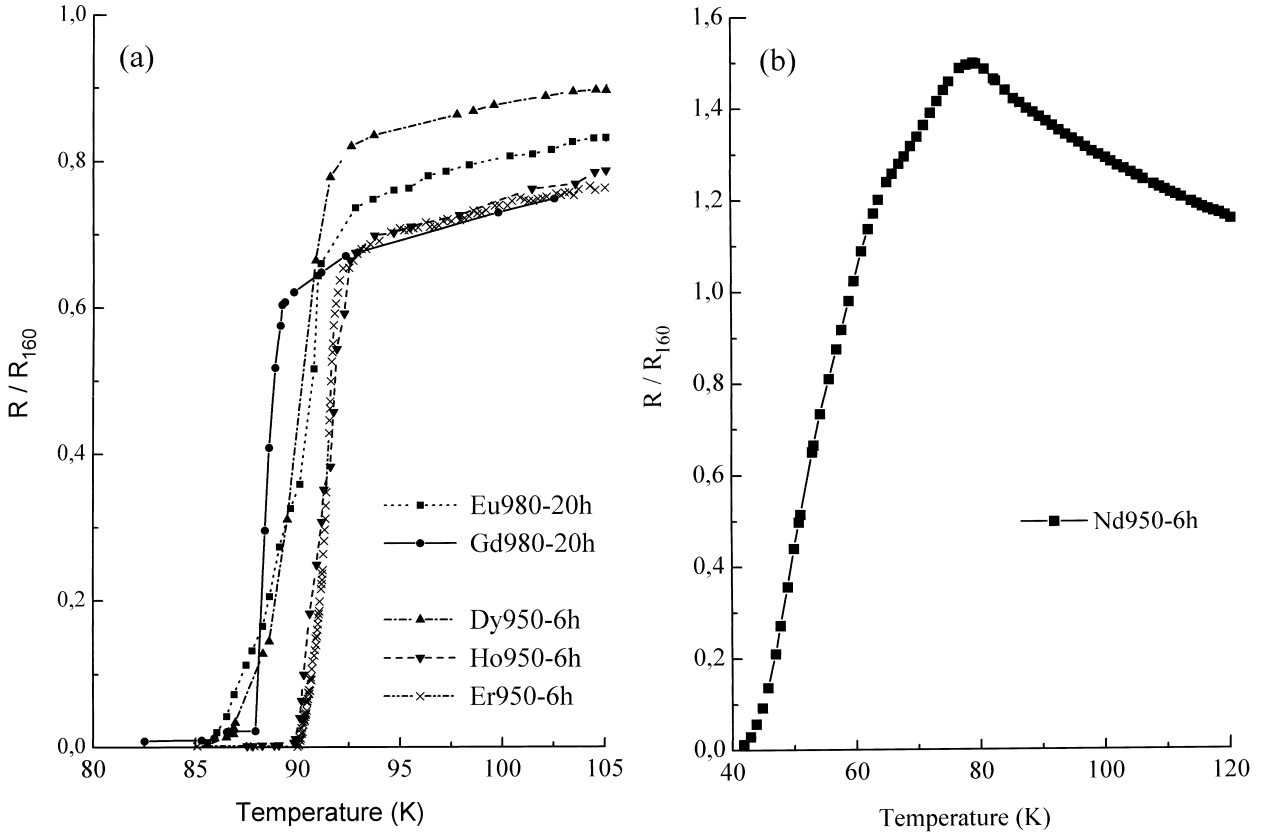

Fig. 12. Electrical resistivity curves of (a) $ReBa_2Cu_3O_y$ (Re = Eu, Gd, Dy, Ho, Er) samples sintered at 950°C for 6 h or at 980°C for 20 h and (b) of $NdBa_2Cu_3O_y$ samples sintered at 950°C for 6 h.

$$CuO + YBa_2Cu_3O_y \leftrightarrow Y_2BaCuO_5 + \text{Liquid} \quad (1)$$

The impurity phase CuO can induce this peritectic reaction even if it is present in amounts undetectable by the X-ray diffraction analysis.[6] It has been also reported by Shin et al.[9] that as the content of CuO is increased, this reaction becomes more prevalent.

In the case of this work, it can be clearly seen in Fig. 2 that XRD analysis detects CuO impurities in all the systems showing this endothermic peak, whereas in the systems NdBCO, GdBCO where DTA results did not show this event, CuO impurities could not be detected. The only exception is ErBCO system in which CuO was not detected by XRD but this DTA peak was present at 954°C. In any case this system contains much higher amounts of impurities and perhaps CuO traces undetectable by XRD.

Combining these results with literature data, the first DTA peak observed in the samples could be attributed to the peritectic reaction (1). Dilatometric results showed that for all the powders the shrinkage starts between 855 and 905°C depending on the powder system. The systems with smaller Re ionic radius, show steeper shrinkage curves and in general lower temperatures of maximum shrinkage rate.

Comparing the shrinkage behaviour of these systems (Table 2), it can be also noticed that there is a dependence of the onset temperature of shrinkage on the ionic radius of the Re ion. Indeed, in the case of higher Re ionic radius (i.e. Nd, Eu, Gd, Dy) systems, the onset is shifted to higher temperatures as the ionic radius increases. The systems of the lowest Re ion size examined, HoBCO and ErBCO, do not comply to the above statement. X-ray diffraction analysis results of the HoBCO powders as already presented (Fig. 2), showed the presence of impurities attributed to incomplete reaction towards the $HoBa_2Cu_3O_y$ phase.[13] This is probably the reason of the delayed start of the densification procedure compared to DyBCO system which shows much higher purity. However, the first peak of the shrinkage rate curve in HoBCO system is observed practically at the same temperature where the peak of DyBCO system appears, although the onset temperature of this curve (start temperature of the shrinkage) is observed at higher temperature (872°C), compared to the temperature of DyBCO system (855°C).

Further investigation of the densification behaviour of HoBCO system was carried out, as already mentioned, by sintering HoBCO samples at 935 and at 955°C followed by abrupt cooling. SEM studies on

these samples after cooling showed the presence of $BaCuO_2$ regions on the samples sintered at 935°C, while these regions were not found after sintering at 955°C, indicating that $BaCuO_2$ impurities have been almost totally reacted towards $HoBa_2Cu_3O_y$ phase. This observation could be a possible explanation of HoBCO densification behaviour. At the initial densification stages $BaCuO_2$ impurities present in the system impose a slow densification rate. At around 950°C where $BaCuO_2$ impurities have almost totally reacted towards $HoBa_2Cu_3O_y$ phase, the densification rate changes become equally rapid as in DyBCO case. The second DTA peak observed in HoBCO system at 970°C, is being attributed either to the eutectic reaction between $HoBa_2Cu_3O_y$ and $BaCuO_2$ traces present in the samples or to the slow decomposition of the $HoBa_2Cu_3O_y$ phase, since as reported in the literature,[13] the $ReBa_2Cu_3O_y$ decomposition occurs at lower temperature as the Re ion size decreases. Indeed, both EDS and XRD studies, as already presented, showed the presence of impurities ($BaCuO_2$ and Re_2BaCuO_5) after sintering at 980°C. Such grains could not be detected in samples sintered at lower temperatures.

Delayed densification compared to DyBCO was also observed on ErBCO system. This powder contains as already discussed, apart from the $ErBa_2Cu_3O_y$ phase, unreacted Er_2BaCuO_5 and $BaCuO_2$ phases in considerable amounts. This system presented also the previously discussed DTA peak at 968°C which is attributed either to the $ErBa_2Cu_3O_y$ eutectic formation with $BaCuO_2$ or to its decomposition. ErBCO system shows also that the densification delays, starting at 865°C, while its maximum rate is observed at the lowest temperature (925°C). However, the densification rate remains low. For temperatures higher than 980°C the ErBCO samples presented a strong shrinkage with a peak at 987°C that is attributed to sample melting.

Concerning density measurements and grain growth studies, the results showed similar dependence on Re ionic radius size. Systems of large Re ionic radius (NdBCO, EuBCO, GdBCO) show slow linear density increase with temperature. As this radius decreases, the densification rate increases. Thus, in all sintering temperatures, the following order occurs: $d_{GdBCO} > d_{EuBCO} > d_{NdBCO}$ (d: % theoretical density). For the other three systems with lower Re radius (DyBCO, HoBCO and ErBCO), the results are different showing an abrupt densification at a temperature depending on the system. The results are in perfect agreement with dilatometric measurements discussed previously. Thus, HoBCO and ErBCO systems that present higher amounts of impurities indicate slower densification rates with densification curves shifted at higher temperatures.

The same behaviour appears also in grain growth results derived from SEM/EDS analysis (Figs. 8–11). The samples of the systems with the higher Re ionic radius: NdBCO, EuBCO and GdBCO, exhibit a normal grain growth. The increase of the sintering temperature enlarges the grains, which in most of the cases appear to have the correct $ReBa_2Cu_3O_y$ stoichiometry. In DyBCO samples sintered at the low temperature of 910°C, needle-like grains were detected by SEM. Some of these grains grow in DyBCO samples upon some unreacted CuO particles and exhibit a stoichiometry close to Dy_2BaCuO_5 phase, which is a result of the peritectic reaction. In HoBCO samples the abrupt increase of grain size observed for temperatures higher than 910°C, is in good agreement with the abrupt increase of sample's density at these temperature conditions and the early densification observed in dilatometric measurements. DyBCO samples have reached their maximum density after sintering at 930°C for 6 h and the density does not change significantly at higher temperatures. However, for temperatures higher than 930°C, a constant increase of the grains is observed. At this temperature the mean grain size has reached the value of 8 μm. A more rapid grain growth was observed between 910 and 930°C, which is also the temperature range of maximum densification rate.

As already discussed, the first endothermic peak observed on the DTA curve at around 960°C, is attributed to the peritectic reaction of the $ReBa_2Cu_3O_y$ phase with CuO present as impurity in the sample. According to Aselage et al.,[6] additional support for this event is derived from densification and grain growth studies as a function of temperature and sample composition. Enhanced transport rates associated with the presence of the liquid phase accelerate the grain growth kinetics and densification rates of $YBa_2Cu_3O_y$ samples. Indeed, enhanced grain growth and densification rates are generally observed when the sintering temperature is close to this peritectic reaction (1). This is exactly the case in DyBCO, HoBCO and ErBCO systems and thus, this phenomenon could explain the abrupt densification and grain growth observed at the first two samples at the low sintering temperature of about 930°C. The considerable amount of impurities present in ErBCO samples had as a result their delayed and slow densification. It seems that the Er_2BaCuO_5 and $BaCuO_2$ grains, present in ErBCO samples, hinder the formation reaction of stoichiometric $ErBa_2Cu_3O_y$ phase. For this reason, up to 960°C, the grain size is not higher than 8.5 μm while at the higher temperature of 970°C the samples are partially glassy. The ErBCO samples sintered for 6 h at the even higher temperature of 980°C consist mainly of large asymmetric or rectangular (18×7 μm) Er_2BaCuO_5 grains (Fig. 11b). Indeed, DTA analysis showed the melting of $ErBa_2Cu_3O_y$ starting at 994°C.

Similar results, concerning uniquely the YBCO system, have been reported by other researchers.[5–11] Chu et al.,[5] studying the grain growth kinetics of YBCO compound,

indicated that at 975°C the grain growth rate is higher than that at 925–950°C due to the formation of a liquid phase at grain boundaries.

The onset and offset temperature of the superconducting transition was used to assess the sample quality. The results of electrical resistivity measurements are shown in Table 3 and in Fig. 12. All the systems (Fig. 12a), with the exception of NdBCO (Fig. 12b), showed high temperature of transition onset (93–95 K) which is very close to the maximum reported values.[15] In addition, the linear temperature dependence of resistivity R and the positive slope of the curve ($\delta R/\mathrm{d}T > 0$) before the onset of superconductivity indicate that the samples under the examined sintering conditions (950°C for the low Re ionic size systems and 980°C for the high Re ionic size systems) are good superconductors. However, the lower value of the offset temperature compared to the onset one and thus the relatively broad width of the transition suggests either the presence of some second phases in the grain boundaries isolating some superconducting grains, or incomplete oxygenation, perhaps due to the high density of samples. Indeed ErBCO and HoBCO samples which had lower density (80 and 90% of the theoretical one, respectively) compared to the other ones exhibited also high offset temperature (~90 K) and thus narrow width of transition range (~3 K).

NdBCO sample, in all cases, was not superconducting above the liquid nitrogen temperature, since the zero resistance temperature was at about 40 K (with onset at about 78 K) as it is shown in Fig. 12b. As it has also been reported,[16–22] the oxygenation of the NdBCO system is very difficult due to the large size of Nd ion and thus it is very difficult to obtain good superconducting properties in this system. There is a significant influence of the Re ion size on the temperature of the orthorhombic/tetragonal transition (O/T transition). From studies on thin films,[20] it has been also reported that as the ionic radius of the rare earth gets larger, the transformation of the tetragonal $ReBa_2Cu_3O_y$ phase to the superconducting orthorhombic one becomes more difficult. The compressional strain of rare earth ions in the barium cage increases with decreasing rare earth ionic radius, forcing an increasing orthorhombic distortion.[21] According to Shaked et al.,[22] the repulsion energy of oxygen atoms in O(1) and O(5) lattice sites in $NdBa_2Cu_3O_y$ is smaller than in $YBa_2Cu_3O_y$ and as a result the lower repulsion energy apparently stabilizes the orthorhombic structure at higher values of y in $NdBa_2Cu_3O_y$ compared to $YBa_2Cu_3O_y$. Prado et al.,[18] by evaluating the temperature of the O/T transition in two systems ($NdBa_2Cu_3O_y$, $GdBa_2Cu_3O_y$) and by comparing them with values of $YBa_2Cu_3O_y$, concluded that the increase of the Re ion size shifts this temperature to lower values. For these reasons the $NdBa_2Cu_3O_y$ samples have to be oxygenated at different temperature than the other systems in order to stabilize the orthorhombic superconducting phase.

5. Conclusions

In this work, a comparison study of the processing conditions for the production of dense $ReBa_2Cu_3O_y$ samples was carried out. Processing conditions for achieving high quality $ReBa_2Cu_3O_y$ samples in terms of purity, density and electrical properties are dependent on the ion size of the central Re ion. Systems with Re > Dy require sintering at increased temperature. Density and mean grain size increase almost linearly with temperature, the systems with the smaller ion size reaching higher values at lower temperatures. The purity of these systems remains rather unaffected by the sintering temperature. For the systems with Re ⩽ Dy, an abrupt increase of density and grain size occurs at a relatively low temperature, specific for each system. The purity of the systems is deteriorated when the firing temperature exceeds 950°C. T_C transition temperatures of the samples processed under the optimum conditions for each system are very close to the maximum reported values.

References

1. Yoo, S. I., Higuchi, T. and Murakami, M., RE–Ba–Cu–O for high functional superconducting permanent magnet. *Mater. Sci. Engin., B*, 1998, **53**, 203–210.
2. Yao, X. and Shiohara, Y., Large REBCO single crystals: growth processes and superconducting properties. *Supercond. Sci. Technol.*, 1997, **10**, 249–258.
3. Yoo, S. I., Nakai, N. and Murakami, M., Melt processing for obtaining $REBa_2Cu_3O_y$ superconductors (RE = Nd, Sm) with high Tc and large Jc. *Ieee Trans. on Appl. Superconductivity*, 1995, **5**(2), 1568–1575.
4. Ferreti, M., Magnoe, E. and Olcese, G. L., Single crystal growth and phase diagram studies in the $REBa_2Cu_3O_y$ systems (R = Y and rare earths). *Physica C*, 1994, **235–240**, 311–312.
5. Chu, C. T. and Dunn, B., Grain growth and the microstructural effects on the properties of YBa_2Cu_3O7-y superconductor. *J. Mater. Res.*, 1990, **5**(9), 1819–1826.
6. Aselage, T. L., Occurrence of free CuO in $YBa_2Cu_3O_{6+\delta}$ and its effect on melting and solidification. *Physica C*, 1994, **233**, 292–300.
7. Baik, S., Moon, J. H., Moon, K. W. and Jang, H. M., A critical comparison of various processing methods for superconducting $YBa_2Cu_3O_{7-x}$ *Ceramic Superconductors II — Research update*, 1988, 186–197.
8. Hill, M. D., Blendell, J. I., Vaudin, M. D. and Chiang, C. K., Processing effects on microstructure and superconducting properties of sintered $YBa_2Cu_3O_{7-x}$. *J. Am. Ceram. Soc.*, 1995, **78**, 1953–1957.
9. Shin, M. W., Kingon, A. I., Hare, T. M. and Koch, C. C., The effects of excess CuO on the grain growth kinetics, sintering and microstructure of the $YBa_2Cu_3O_{7-\delta}$ superconductor. *Mater. Letters*, 1992, **15**, 13–18.
10. Chu, C. T. and Dunn, B., Grain growth and the microstructural properties of $YBa_2Cu_3O_{7-y}$ superconductor. *J. Mater. Res.*, 1990, **5**, 1819–1826.

11. Clarke, D. R., Shaw, T. M. and Dimos, issues in the processing of cuprates ceramic superconductors. *J. Am. Ceram. Soc.*, 1989, **72**, 1103–1113.
12. Stepien-Damm, J., Rogacki, K., Morawska-Kowal, T. and Damm, Z., Modified synthesis of superconducting single phase and high density (Re)Ba_2Cu_3O7 samples. *Supercond. Sci. Technol.*, 1992, **5**, 346–348.
13. Andreouli, C. and Tsetsekou, A., Synthesis of HTSC Re(Y)Ba_2Cu_3Ox powders: the role of ionic radius. *Physica C*, 1997, **291**, 274–286.
14. Gotor, F. J., Fert, A. R., Odier, P. O. and Pellerin, N., Grain growth, microstructure, and superconducting properties of pure and Y2BaCuO$_5$-doped $YBa_2Cu_3O_{7-x}$ ceramics. *J. Am. Cerm. Soc.*, 1995, **78**, 2113–2121.
15. Tarascon, J. M., McKinnon, W. R., Greene, L. H., Hull, G. W. and Vogel, E. M., Oxygen and rare earth doping of the 90-K superconducting perovskite $YBa_2Cu_3O_{7-x}$. *Phys. Rev. B*, 1987, **36**, 226–234.
16. MacManus-Driscoll, J. L., Alonso, J. A., Wang, P. C., Geballe, T. H. and Bravman, J., Studies of structural disorder in $ReBa_2Cu_3O_{7-x}$ thin films (Re = rare earth) as a function of rare-earth ionic radius and film deposition conditions. *Physica C*, 1994, **232**, 288–308.
17. Schneemeyer, L. F., Waszczak, J. V., Zaborak, S. M., van Dover, R. B. and Siegrist, T., Superconductivity in rare earth cuprate superconductors. *Mater. Res. Bul.*, 1987, **22**, 1467–1473.
18. Prado, F., Caneiro, A. and Serquis, A., High temperature thermodynamic properties, orthorhombic/tetragonal transition and phase stability of $GdBa_2Cu_3O_y$ and related R123 compounds. *Physica C*, 1998, **295**, 235–246.
19. Tang, M. I., Leelaprute, S. and Winotai, P., Rare earth ion size effect in the rates of suppression of the TC's of the 'Re123' high-temperature superconductors due to magnetic ion substitution into the Cu(2) sites. *Physica C*, 1999, **312**, 321–326.
20. Yoo, S. I., Sakai, N., Takaichi, H., Higuchi, T. and Murakami, M., Melt processing for obtaining $NdBa_2Cu_3O_y$ superconductors with high T c and large J c. *Appl. Phys. Lett.*, 1994, **65**, 633.
21. Ramesh, S. and Hedge, M. S., Bond-valence analysis of the charge distribution and internal stresses in the $ReBa_2Cu_3O_{7-\delta}$ system (R = rare earth). *Physica C*, 1994, **230**, 135–142.
22. Shaked, H., Veal, B. W., Faber, J., Hitterman, R. L., Balachandran, U., Tomlins, G., Shi, H., Morss, L. and Paulikas, A. P., Structural and superconducting properties of oxygen-deficient $NdBa_2Cu_3O_{7-\delta}$. *Phys. Rev. B*, 1990, **41**, 4173–4179.